Noncrystalline Phases in Poly(9,9-di-*n*-octyl-2,7-fluorene)

S. H. Chen and A. C. Su*

Institute of Materials Science and Engineering and Center for Nanoscience and Nanotechnology, National Sun Yat-sen University, Kaohsiung 804, Taiwan

S. A. Chen

Department of Chemical Engineering, National Tsing Hua University, Hsinchu 300, Taiwan

Received: December 29, 2004; In Final Form: March 23, 2005

Selective formation of amorphous, nematic (N), and β phases in poly(9,9-di-*n*-octyl-2,7-fluorene) (PFO) films was achieved via judicious choice of process parameters. Phase structure and film morphology were carefully examined by means of X-ray diffraction as well as electron microscopy. "Amorphous" thin films were obtained by quick evaporation of solvent. Slow solvent removal during film formation or extended treatment of the amorphous film with solvent vapor resulted in predominantly the β phase, which corresponds to a frozen (due to decreased segmental mobility upon solvent removal) and intrinsically metastable state of transformation midway between a solvent-induced clathrate phase and the equilibrium crystalline order in the undiluted state. The frozen transformation process is reactivated upon an increase in temperature beyond 100 °C. Compared to the amorphous film, extended backbone conjugation in the β phase is evidenced from the emergence of a characteristic absorption peak around 430 nm near the absorption edge. For films of frozen nematic order (obtained by quenching from the nematic state), the conjugation length is also greater than the amorphous films as revealed by an absorption shoulder around 420 nm. Well-behaved single-chromophore emission with single-mode phonon coupling was observed for the β phase; in the case of nematic films, dual-mode phonon coupling must exist if single-chromophore emission is assumed. In comparison, the emission spectrum of the amorphous film of generally shorter conjugation lengths exhibited mixed characteristics of nematic and β phases, implying the presence of minor populations of extended conjugation similar to those in nematic and β phases, which are of biased weightings in the emission spectra. All these films consist of nanograins (ca. 10 nm in size) of collapsed chains; the films are therefore inherently inhomogeneous in this length scale. In combination with previous observations on the crystalline (α and α') forms, the phase behavior of PFO is then generally summarized in terms of relative thermodynamic stability.

Introduction

As one of the most extensively studied examples of semiconducting polymers,[1−3] poly(9,9-di-*n*-octyl-2,7-fluorene) (PFO, chemical structure given as inset in Figure 3b) is well-known to be crystalline with a melting temperature around 160 °C, above which a nematic (N) mesophase exists up to ca. 300 °C.[4−7] There may also be a mesomorphic β phase upon solvent vapor treatment.[8,9] As these phases can be rather selectively maintained via proper selection of processing parameters,[4,8,9] the resulting "morphological effects" in light-emission properties have been extensively examined in the literature.[10−19] However, details of molecular arrangement, morphological features, and transformation paths in these phases remained incompletely explored,[9,18] rendering earlier attempts to establish correlation between morphology and photophysical properties rather imprecise.

As one of the systematic efforts to clarify the phase behavior of PFO, we have recently proposed a structural model for the α phase as orthorhombic (a = 2.56 nm, b = 2.34 nm, c = 3.32 nm, space group $P2_12_12_1$) with eight chains in the unit cell (each of four fluorene repeats) on the basis of transmission electron microscopy (TEM) and X-ray diffraction (XRD) observations.[20] We have further reported[21] the presence of a previously unspecified crystalline form, which is closely related to the α

form (hence coined as the α' phase) and is kinetically favored at crystallization temperatures below ca. 130 °C. The modification involves mainly the lowered symmetry along the *b*-axis and a slight increase in its dimension to 2.38 nm, in addition to the interesting habit of preferential orientation of the *a*-axis along the film normal. This oriented α' form exhibits a stronger red shift of the absorption edge than the α phase, as compared to the nematic "blank" comprising only the nematic phase. In contrast, optical emission of the α' film (containing the α' phase in a nematic matrix) remains highly similar to those of the α film (containing the α' phase in a nematic matrix) and the nematic "blank", suggesting that the crystalline phases contribute little to photoexcited emission of PFO films. In other words, optical emission of PFO films is dominated by the noncrystalline phases.

To complete the picture, we demonstrate here the controlled formation of the noncrystalline (including amorphous, nematic, and β) phases in PFO films. Structural features of these films are carefully characterized by means of TEM and XRD. These are then related to the corresponding optical absorption and photoexcited emission behavior. In combination with previous results for crystalline (α and α') phases, the phase behavior of PFO is then generally summarized with special emphasis on the kinetic routes of phase transformation, which are of crucial

significance in morphological control and its subsequent effects on photooptical properties of PFO films.

Experimental Section

Material and Instruments. The PFO sample used here was purchased from American Dye Source, Quebec, Canada (Catalog No. ADS129BE). The weight-average molecular mass (M_w) was 24 kDa (polydispersity index PDI = 2.6), as corrected from polystyrene-equivalent values on the basis of small-angle light scattering results of Grell et al.[8] Instrumental details concerning transmission electron microscopy (TEM), field-emission scanning electron microscopy (FE-SEM), X-ray diffraction (XRD, Cu Kα line), optical absorption (UV−vis) and photoluminescence (PL) spectroscopies, and differential scanning calorimetry (DSC) were similar to those given previously.[20,21] Polarized light microscopic (PLM) observations were made by use of a Nikon Eclipse E400-POL microscope equipped with an ice water cooled high-temperature stage (Linkman THMS-600, connected to a TMS-91 temperature controller) under protective nitrogen atmosphere.

Film Casting. Two types of film casting procedures were used. We generally adopt the simple drop-cast procedure similar to those adopted in previous studies using dilute solutions (generally ca. 0.1 w/v % or lower for TEM specimens and 0.2 w/v % for other studies) of PFO in toluene on glass or quartz substrates. However, for the preparation of the "amorphous" films used for our UV−vis/PL studies here, a "flow-cast" procedure was adopted, in which the dropped solution was allowed to flow by immediately holding the substrate nearly vertical under a stream of fresh air. This latter procedure results in quick formation of thinner films that appear dark under polarized light and were hence considered "amorphous".

Heat/Vapor Treatment. The as-cast films were then routinely vacuum-dried (in excess of 4 h at ca. 80 °C) before further heat treatments at elevated temperatures. Specimens composed of predominantly the β phase were prepared by either slow solvent evaporation of thick films for XRD studies or, in a more strictly controlled manner, extended treatment of the amorphous film with saturated toluene vapor. Nematic films were prepared by quenching from 250 °C directly into ice water.[22] All heat treatments were made using the PLM high-temperature stage under protective nitrogen atmosphere.

Electron Microscopic Specimens. TEM specimens were detached from the glass substrate using a dilute HF solution. In the case of oriented specimens, a manual shearing procedure (i.e., sweeping a blade over the melted film at 250 °C) was adopted prior to quenching to 0 °C for nematic films (and the subsequent toluene vapor treatment for β films). These specimens were then vapor-deposited with carbon or shadowed (with an incidence angle of 60° from the plane normal) with a combined Pt/C source prior to TEM examinations. FE-SEM specimens were prepared by direct sputter coating with gold without detachment of PFO films from the substrates.

Results and Discussion

Formation of the β Phase. Demonstrated in Figure 1 are PLM observations of the film formation process upon solvent evaporation. The drop-cast liquid film was initially dark (not shown); within a few seconds, a birefringent band emerged near the edge of the liquid film (Figure 1a). The birefringent band subsequently developed further inward (Figure 1b), but the process ended rather quickly (within 1 min, Figure 1c). Subsequent observations (Figure 1d) showed no further development of this birefringent band, suggesting that the thinner
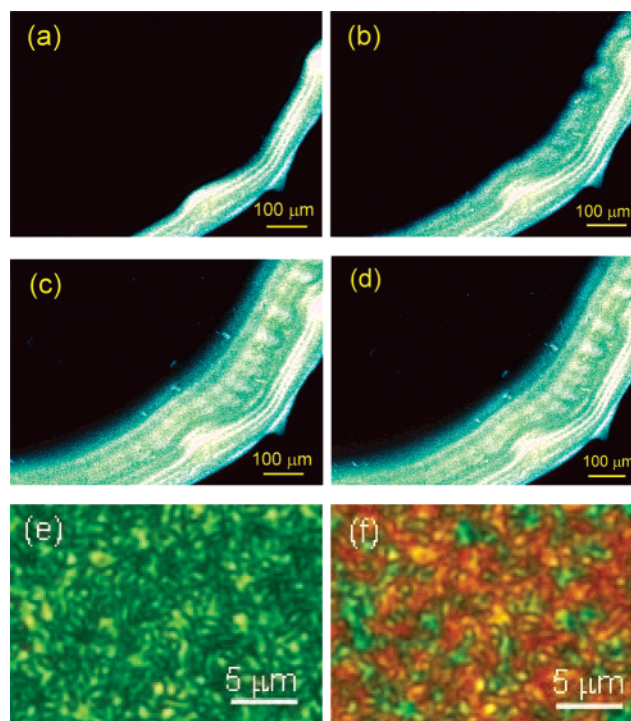
Figure 1. Sequence of PLM micrographs showing emergence of β phase upon solvent evaporation during film formation via drop casting from a 0.2% toluene solution. Note that clear birefrigence is observed only in the rim region of greater thickness (i.e., the "coffee stain" effect), where it takes a longer time to dry. This indicates kinetic effects in the formation of β phase. The thin, quickly dried (upper left) region without discernible optical anisotropy is considered "amorphous". The entire process for the β phase to form as a band near the rim (extending from the upper right corner to the lower central part of the micrographs) is completed (a−c) within ca. 1 min; additional time of observation showed no further changes in the optical texture (d). Magnified views of a more completely developed β film (via extended toluene vapor treatment at room temperature) demonstrate the domain-wall texture (e) under cross polarities and (f) with gypsum plate inserted.

interior of the as-cast film remained optically isotropic and was hence considered amorphous. It should be noted that repeated droppings of solution on top of the film result in better developed birefringent features in regions that were initially amorphous. Extended treatment with toluene vapor at room temperature may also result in better developed β phase. Figure 1e,f exhibits details of the domain-wall texture under higher magnification.
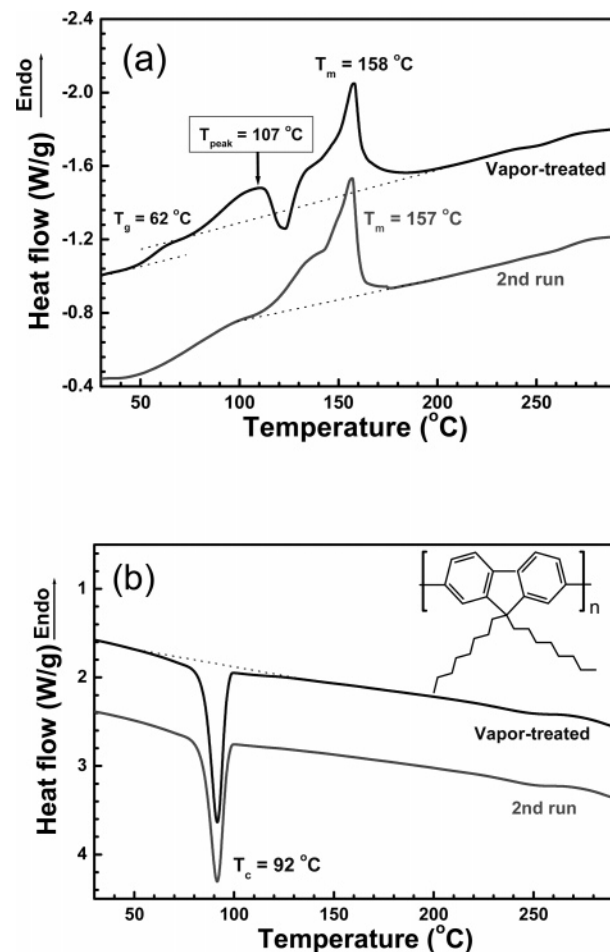
Given in Figure 2a are a series of representative in situ XRD profiles obtained during film formation. As the film was still "wet" (bottom curve), there were already features of ordered structure indicated by a series of clearly discernible peaks; among them, the most prominent one is located at $2\theta = 7.0°$, ca. 1.28 nm in d spacing which coincides with the (200) reflection of crystalline PFO. However, one cannot attribute this ordering to either α or α′ crystallites as other reflections in the corresponding XRD profiles do not match.[20,21] It is more likely that this is related to a certain solvent-induced clathrate phase. This attribution is supported by further observations that reflections of the initial structure broadened and shifted in position upon continued removal of solvent; the new location of the prominent low-angle peak (middle curve) corresponds to a decreased d spacing value of 1.21 nm. After continued vacuuming for 4 h, there are only four broad reflections left in the XRD profile (upper curve), with corresponding d spacing values of 1.22, 0.87, 0.61, and 0.44 nm. The observation of decreased sharpness of reflections during film formation indicates that the (presumed) clathrate structure is unstable with

Noncrystalline Phases of PFO

J. Phys. Chem. B, Vol. 109, No. 20, 2005 **10069**
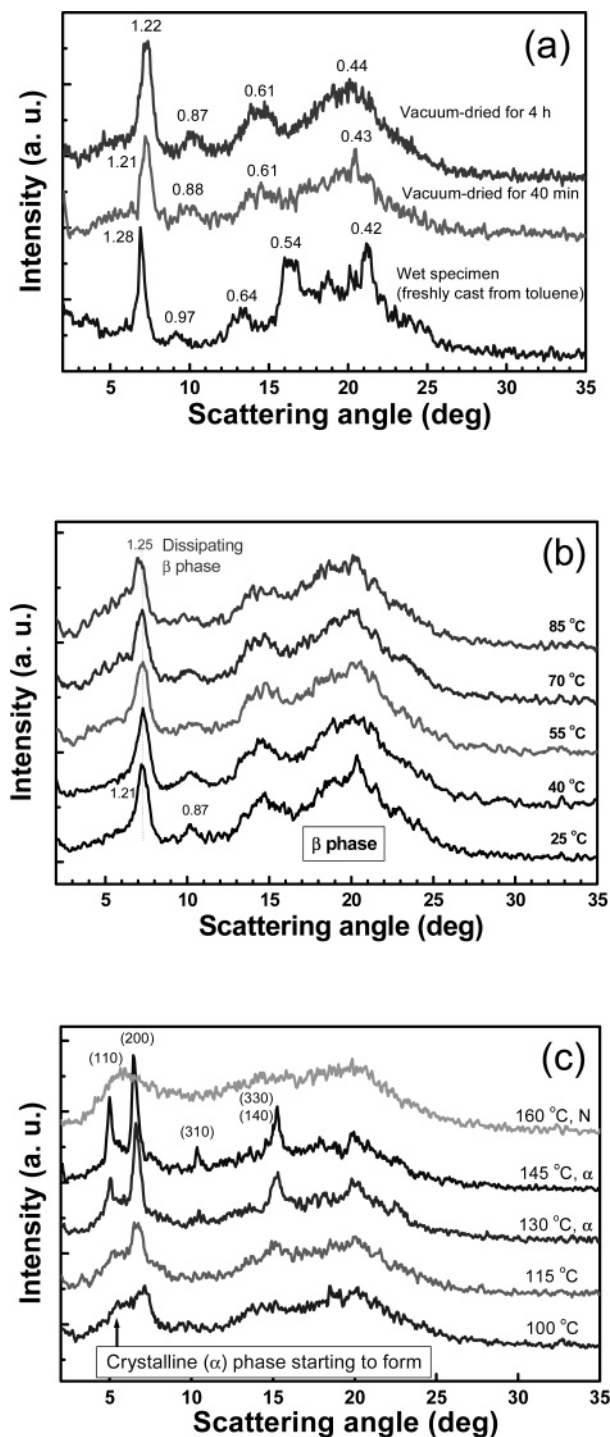
Figure 2. Wide-angle X-ray diffraction profiles showing (a) emergence of β phase during film formation upon drying from the wet film state in the vacuumed sample stage, (b) sustained β structure up to 85 °C, and (c) partial dissipation of β order at 100 °C, transformation into crystalline (α) order above 115 °C, as well as final melting into nematic phase at 160 °C in a sequence of measurements at stepwise increased temperatures in intervals of 15 °C. Data collection for each profile took ca. 40 min to complete.

Figure 3. (a) Heating and (b) cooling DSC traces showing dissipation of β phase above 80 °C and subsequent transformation into α phase that melts near 160 °C. Note that the β phase does not recover upon cooling as indicated by the absence of its dissipation/reorganization in the second heating trace.

further decrease in solvent concentration and tends to transform into crystalline order,[21] but the process is inhibited by the corresponding decrease in segmental mobility. This β phase of intermediate order should therefore be intrinsically metastable, as is indeed confirmed in the following observations.

Metastability and Transformation of the β Phase. With stepwise increases in intervals of 15 °C, XRD profiles in Figure 2b,c demonstrate initial dissipation of mesomorphic order at

85 °C, subsequent recrystallization and perfection of the crystalline order at 100 °C or higher, and final melting into nematic order above at 160 °C. These observations are consistent with the DSC heating trace of toluene vapor treated film in Figure 3a, in which the endotherm above 80 °C coincides with the dissipation of β phase whereas the following exotherm around 120 °C corresponds to the attributed recrystallization. The perfected crystalline order involves certainly the α phase, as indicated by the characteristic presence of (110) and (310) reflections in Figure 2c. Simultaneous presence of the low-melting α′ form (which is kinetically favored at low crystallization temperatures but tends to reorganize into the α form upon reheating)[21] in the early stage of transformation is also likely. This is indicated by the increases in intensities of (110) and (310) reflections relative to the (200) peak in the temperature range of 115−145 °C.

The attribution above is also supported by the presence of the endothermic shoulder near 140 °C before the final melting at 158 °C in the DSC first heating trace Figure 3a. In this particular case, the sample film was further toluene vapor treated after drop casting and to ensure dominance of the β phase before DSC analysis. As noted previously,[21] reorganization of the α′ phase (formed typically around 90 °C during programmed cooling; cf. also the cooling traces in Figure 3b) into the α form is quite generally observed around 140 °C upon subsequent reheating (cf. also the first-run and second-run heating traces in Figure 3a). It may therefore be concluded that the β phase is
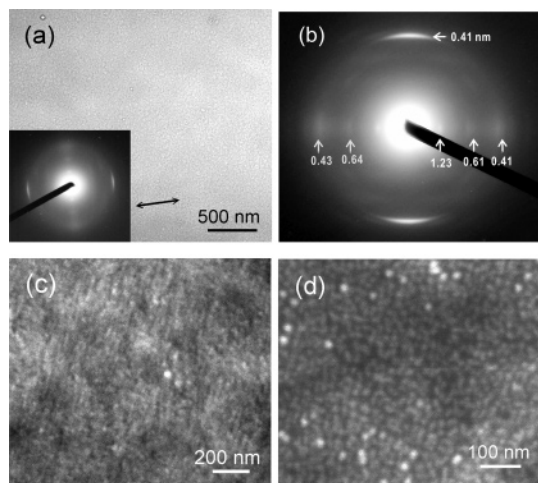
Figure 4. (a) BFI and corresponding SAED pattern of β phase. Specimen sheared at 250 °C, quenched to 0 °C, followed by toluene vapor treatment for 64 h. Double-headed arrow indicates corresponding shear direction. (b) Expanded SAED pattern with shear direction along the meridian, (c) SEI showing features of aligned nanograins, and (d) highly magnified SEI for clearer identification of nanograins.

generally metastable, which transforms into crystalline (α' and α) phases upon subsequent increases in temperature before final melting of crystalline order into nematic melt near 160 °C. We emphasize here that the formation of β phase requires the presence of absorbed solvent: the mesomorphic order, once dissipated upon heating, does not recover during subsequent cooling.

Structural/Morphological Features of the β Phase. In contrast to shear-oriented α and α' films which tend to be banded along the shear direction,[21] the shear-oriented β films appear generally homogeneous, as indicated by the representative bright-field image (BFI) in Figure 4a, where the corresponding selected-area electron diffraction (SAED) pattern indicates backbone alignment along the shear direction. Magnified view of the SAED pattern (shear direction lying along the meridian) in Figure 4b is in general consistent with the XRD fiber pattern reported by Grell et al.[9] The strong meridional arc corresponds to a d spacing value of 0.42 nm, which is commensurate with half of the monomeric repeat or interphenylene spacing along the backbone. Equatorial arcs with d spacing values in commensuration of lamellar structure with layer spacing of 1.23 nm may be identified. Additional yet diffuse equatorial arcs with d spacing values around 0.64 and 0.43 nm may also be identified, indicating additional in-plane order. These are all consistent with our interpretation that the so-called β phase is of transient nature, i.e., at an intermediate stage (frozen by the decreased segmental mobility due to solvent removal) of transformation from the solvent-induced clathrate structure to the solvent-free crystalline order.

Representative surface topographic features of β films are shown in Figure 4c. Nanograins approximately 10 nm in size may be identified. Similar observations of the nanograin features have previously been reported for crystalline PFO[21] as well as mesomorphic poly(1,4-phenylenevinylene) (PPV) derivatives[23−25] and have been qualitatively discussed in terms of collapsed chains (upon simultaneous cooling and solvent removal) during film formation on the basis of Flory's classical theory[26] of lyotropic liquid crystallinity for rodlike polymers.

Morphological Features of Amorphous and Nematic Films. As nanograins are attributed to the collapse of chains during film formation, one would expect corresponding features in the as-cast film as well. This is indeed observed in the case
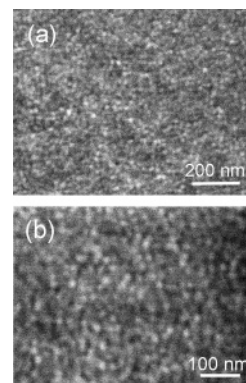

Figure 5. (a) Representative secondary electron image (SEI) of amorphous (as flow cast) specimens, showing the randomly arranged nanograins and thin cracks that are more clearly identifiable in (b) the blowup view.
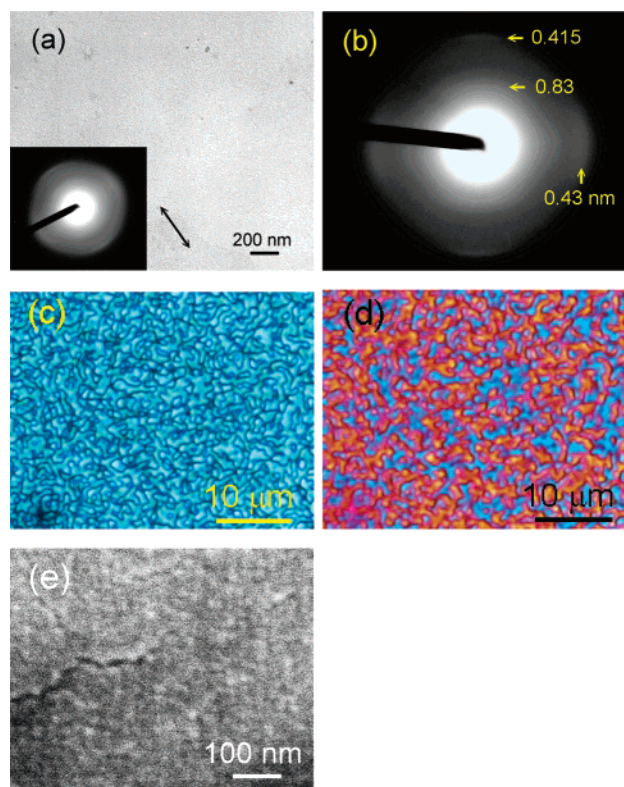
Figure 6. (a) Representative BFI and corresponding SAED pattern of the nematic specimen sheared at 250 °C followed by quenching in ice water. Double-headed arrow indicates shear direction. (b) Expanded view of the SAED pattern, where shear direction lies along the meridian. Cross-polarized optical micrographs of the nematic film, showing (c) Schlieren-like features under cross polarities and (d) domain-wall texture upon insertion of gypsum plate. (e) Representative SEI of flow-cast nematic specimen heated to and quenched from 250 °C, showing weakly coalesced nanograins and presence of fine cracks.

of amorphous films, as demonstrated in Figure 5. It should be noted that the amorphous nature of these as-flow-cast films has been further confirmed by the corresponding featureless SAED patterns (not shown here). Although not as clearly discernible as in the case of β or amorphous films, features of nanograins may also be identified in the case of nematic films quenched from 250 °C (Figure 6e). All the above observations are consistent with the proposed picture of collapsed chains.

The nematic order stated above for films quenched from 250 °C is supported by TEM observations shown in Figure 6a,b. In the magnified SAED pattern (Figure 6b), one may observe

Noncrystalline Phases of PFO

J. Phys. Chem. B, Vol. 109, No. 20, 2005 **10071**
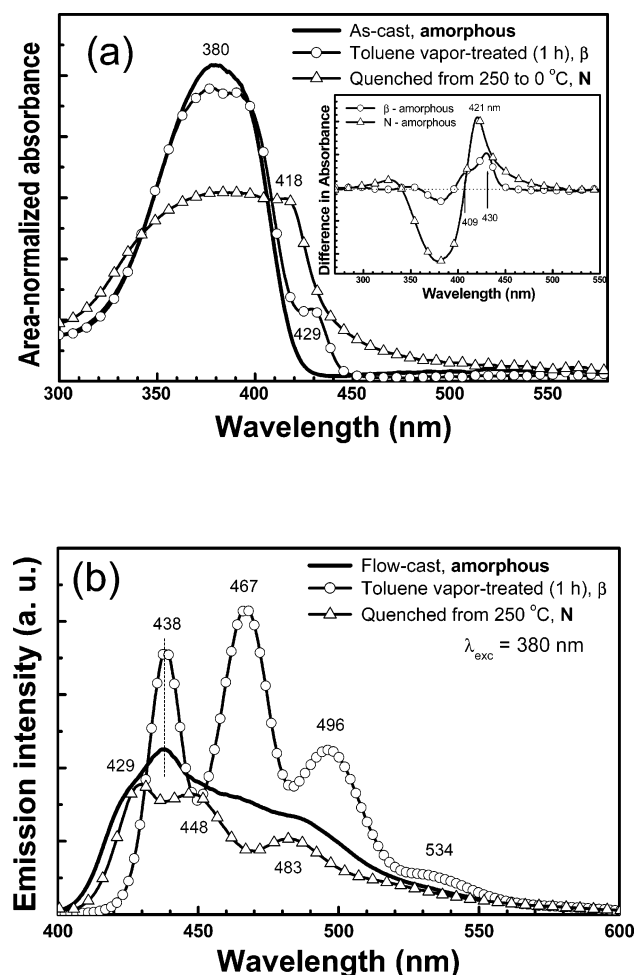
Figure 7. (a) Optical absorption of the flow-cast (as-cast, largely amorphous), toluene vapor treated (β phase), and quenched (from 250 °C, nematic) films. Difference spectra after subtraction of the amorphous glass spectrum are shown in the inset. (b) Corresponding emission spectra, showing clearly red-shifted emission maxima of the β phase. Note that the emission maximum of the "amorphous" film carries characteristics of both β and N phases.

meridional reflections corresponding to the monomeric repeat of 0.83 nm; the fact that the second-order reflection is stronger and sharper than the first-order counterpart implies *approximate* 2_1 conformation along the backbone. The weak and broad equatorial reflection centered around 0.43 nm in d spacing may be attributed to interchain spacing. These are in general agreement with an earlier XRD fiber pattern obtained by Grell et al.,[9] except that they observed an additional equatorial reflection of 1.6 nm in d spacing, leading to a postulated packing of ribbons ca. 1.6 nm width and 0.44 nm thickness. We attribute the absence of this particular equatorial reflection to dynamic effects of electron diffraction. Consistent with the assignment of nematic ordering, PLM micrographs given in Figure 6c (cross polarities) and Figure 6d (gypsum plate inserted) demonstrate fine Schlieren-like features and domain-wall texture, respectively, in a manner similar to that of earlier cases of hairy-rod polyamides and polyesters of sanidic liquid crystallinity.[27,28]

Optical Absorption. Area-normalized absorption spectra of films of various phases are compared in Figure 7a. For the as-cast amorphous film, the main absorption centers around 380 nm, with a red edge located near 420 nm. Upon toluene vapor treatment, there emerges an additional absorption peak at ca. 430 nm, which has been known to be characteristic of β phase.[9] Nevertheless, a similar peak near 420 nm may also be identified

for the nematic film prepared by direct quenching to 0 °C after a brief (i.e., 5 min) heat treatment at 250 °C. Hence, one may qualitatively state that backbone conjugation is most extended in the β phase and most limited in the amorphous film, whereas the nematic phase serves as an intermediate case between the two.

This redistribution in conjugation length is quantitatively identified in the difference spectra (using the absorption spectrum of the amorphous film as a common base) given in the inset of Figure 7a. Accompanying the transformation of β phase from the amorphous film, there is a general increase in conjugation length, resulting in a minimum near 380 nm and a maximum near 430 nm in the difference spectrum. There is also a secondary maximum in the vicinity of 410 nm, indicating that the extension in conjugation length is in fact bimodal. It should be emphasized here that the "characteristic" absorption peak of the β phase at 430 nm is in fact not so characteristic: a similar absorption maximum in the same wavelength range has been identified for a modification of the crystalline phase (α'). For the nematic film, the relative increase in conjugation length is indicated in the difference spectrum by the minimum centered at 375 nm and a maximum at 420 nm with a long-wavelength tail. This increase in conjugation length is attributed to better coplanarity of backbone rings at elevated temperatures, which was frozen-in during quenching. It is perceivable that the actual level of frozen-in coplanarity depends inevitably on the residence time (i.e., the extent of thermal equilibration of backbone conformation) at the selected heat-treatment temperature (250 °C here) and the effective cooling rate (i.e., the effective frozen-in temperature) during quenching.

Photoexcited Emission. As given in Figure 7b, PL spectrum of the β film exhibits typical vibronic features with the 0−0 transition located at 438 nm (i.e., a Stokes shift of only 8 nm if we assume that the effective emitting species correspond to segments absorbing at 430 nm) and phonon sidebands at 467 and 496 nm. This is consistent with the coupling of a single phonon mode of ca. 1330 ± 80 cm^{-1}, attributable to aromatic ring stretching. We note that the apparently nonmonotonic variation in relative peak intensities in the vibronic structure is not necessarily attributable to a large value[29] of the Huang−Rhys factor and is at least partly related to reabsorption effects, as it depends on film thickness.[21]

For the nematic film, emission peaks located at 429, 448, and 483 nm are identified, with again a small Stokes shift of 8 nm in the 0−0 transition. These observations suggest dual-mode coupling at phonon frequencies of ca. 990 (C═C−H in-plane deformation) and 1300 cm^{-1}, as previously proposed by Ariu et al.[12,16] Interestingly, despite the generally shorter conjugation length, the emission spectrum of the amorphous film exhibits emission features of both nematic and β films. This implies the presence of fine (below PLM resolution) nematic and β domains dispersed within the amorphous matrix. These finely dispersed N or β domains, however, are heavily weighted in the emission spectrum, presumably through efficient energy transfer processes. Similar observations of biased weightings in emission behavior of heterogeneous films have been reported previously for PPV derivatives.[23−25]

As it has been established[21] that the crystalline phase of PFO does not contribute significantly to photoexcited emission of PFO films, one sees that the emission behavior of the β phase is unique among various phases of PFO: it is strongly coupled to the aromatic C═C stretching in the backbone and is comparatively high in PL efficiency. The former is likely related to the high backbone coplanarity in its nearly 2_1 helical
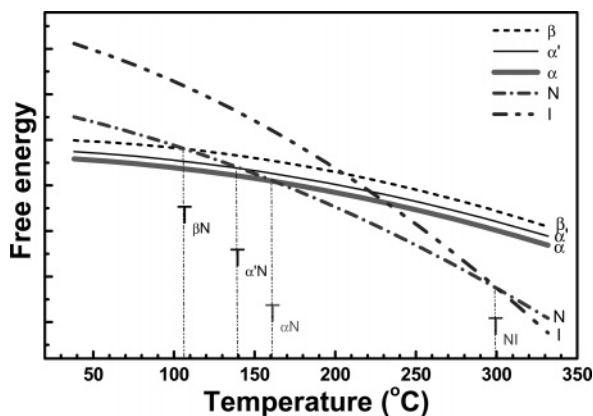
Figure 8. Schematic free energy diagram, showing relative thermodynamic stability of various phases in PFO.

conformation. The latter is qualitatively identifiable from the unnormalized PL spectra in Figure 7b, which correspond to the same piece of film but are different in phase structure via control of the processing parameters.

Summary of Phase Behavior of PFO. By combining our previous observations on crystalline forms and current results on noncrystalline phases, the phase behavior of PFO is summarized via the schematic free energy diagram shown in Figure 8. Experimentally observed temperatures of transformation between phases are indicated, with the direction of phase change (i.e., the relative phase stability) represented by different levels of free energy. We emphasize here that the formation of β phase requires strictly the presence of absorbed solvent. This frozen-in structure, the β phase, as an intermediate stage of transformation midway from a (not yet fully characterized) solvent-induced clathrate structure toward the solvent-free crystalline phase, is inherently unstable: once dissipated upon heating, it does not recover without the presence of solvent.

As a practical guide for preparing β phase specimens via solvent vapor treatment, it should be noted that, in the presence of crystalline (α or α') phase, the conversion toward the β structure is inefficient: the crystalline domains serve as hindrance to solvent diffusion and, in the practical case of low concentration of absorbed solvent, transformation from solvent-free crystals to the clathrate phase is not thermodynamically favored. Our β phase specimens were all prepared using either amorphous or nematic films.

Concluding Remarks

In conclusion, we have shown that the β phase of PFO corresponds to a frozen-in structure en route transformation from a solvent-incorporated clathrate phase to the solvent-free crystalline structure. We have also reaffirmed the dominant presence of nanograins (ca. 10 nm in size) in the PFO films in a manner similar to or clearer than other conjugated polymers previously studied. The inherent morphological heterogeneity in this length scale should in general be relevant to the charge carrier transport and electroluminescence behavior of semiconducting polymer films. This calls for further experimental scrutiny. A summary of the phase behavior of PFO is given schematically in terms of relative free energy, which may serve as a preliminary guide for potential investigators interested in this "fruit fly" of semiconducting polymers. We note further that it would be interesting to examine further differences in chemical stability or mechanical strength of the films upon phase transformation, but these are beyond the scope of the present work.

References and Notes

(1) Kraft, A.; Grimsdale, A. C.; Holmes, A. B. *Angew. Chem., Int. Ed.* **1998**, *37*, 402.

(2) Neher, D. *Macromol. Rapid Commun.* **2001**, *22*, 1365.

(3) Scherf, U.; List, E. J. W. *Adv. Mater.* **2002**, *14*, 477.

(4) Grell, M.; Bradley, D. D. C.; Inbasekaran, M.; Woo, E. P. *Adv. Mater.* **1997**, *9*, 798.

(5) Teetsov, J.; Fox, M. A. *J. Mater. Chem.* **1999**, *9*, 2117.

(6) Blondin, P.; Bouchard, J.; Beaupre, S.; Belletete, M.; Durocher, G.; Leclerc, M. *Macromolecules* **2000**, *33*, 5874.

(7) Kawana, S.; Durrell, M.; Lu, J.; Macdonald, J. E.; Grell, M.; Bradley, D. D. C.; Jukes, P. C.; Jones, R. A. L.; Bennett, S. L. *Polymer* **2002**, *43*, 1907.

(8) Grell, M.; Bradley, D. D. C.; Long, X.; Chamberlain, T.; Inbasekaran, M.; Woo, E. P.; Soliman, M. *Acta Polym.* **1998**, *49*, 439.

(9) Grell, M.; Bradley, D. D. C.; Ungar, G.; Hill, J.; Whitehead, K. S. *Macromolecules* **1999**, *32*, 5810.

(10) Redecker, M.; Bradley, D. D. C.; Inbasekaran, M.; Woo, E. P. *Appl. Phys. Lett.* **1999**, *74*, 1400.

(11) Lee, J. I.; Klaerner, G.; Miller, R. D. *Synth. Met.* **1999**, *101*, 126.

(12) Ariu, M.; Lidzey, D. G.; Bradley, D. D. C. *Synth. Met.* **2000**, *111−112*, 607.

(13) Herz, L. M.; Phillips, R. T. *Phys. Rev. B* **2000**, *61*, 13691.

(14) Cadby, A. J.; Lane, P. A.; Mellor, H.; Martin, S. J.; Grell, M.; Giebeler, C.; Bradley, D. D. C.; Wohlgenannt, M.; An, C.; Vardeny, Z. V. *Phys. Rev. B* **2000**, *62*, 15604.

(15) Ariu, M.; Lidzey, D. G.; Lavrentiev, M.; Bradley, D. D. C.; Jandke, M.; Strohriegl, P. *Synth. Met.* **2001**, *116*, 217.

(16) Ariu, M.; Lidzey, D. G.; Sims, M.; Cadby, A. J.; Lane, P. A.; Bradley, D. D. C. *J. Phys.: Condens. Matter* **2002**, *14*, 9975.

(17) Korovyanko, O. J.; Vardeney, Z. V. *Chem. Phys. Lett.* **2002**, *356*, 361.

(18) Winokur, M. J.; Slinker, J.; Huber, D. L. *Phys. Rev. B* **2003**, *67*, 184106.

(19) Khan, A. L. T.; Banach, M. J.; Köhler, A. *Synth. Met.* **2003**, *139*, 905.

(20) Chen, S. H.; Chou, H. L.; Su, A. C.; Chen, S. A. *Macromolecules* **2004**, *37*, 6833.

(21) Chen, S. H.; Su, A. C.; Su, C. H.; Chen, S. A. *Macromolecules* **2005**, *38*, 379.

(22) We believe that heat treatment at 250 °C is sufficient for erasing all previous thermal histories. A combination of small-angle X-ray scattering (SAXS) and DSC results indicated a maximum level of crystallinity around 40% as well as an estimated (via Gibbs−Thomson approach) value of ca. 185 °C for the equilibrium melting temperature.

(23) Chen, S. H.; Su, A. C.; Chou, H. L.; Peng, K. Y.; Chen, S. A. *Macromolecules* **2004**, *37*, 167.

(24) Chen, S. H.; Su, A. C.; Han, S. R.; Chen, S. A.; Lee, Y. Z. *Macromolecules* **2004**, *37*, 181.

(25) Chen, S. H.; Su, C. H.; Su, A. C.; Chen, S. A. *J. Phys. Chem. B* **2004**, *108*, 8855.

(26) Flory, P. J. *Proc. R. Soc. London* **1956**, *A234*, 73.

(27) Ebert, M.; Herrmann-Schönherr, O.; Wendorff, J. H. *Makromol. Chem. Rapid Commun.* **1988**, *9*, 445.

(28) Watanabe, J.; Harkness, B. R.; Sone, M.; Ichimura, H. *Macromolecules* **1994**, *27*, 507.

(29) Pope, M.; Swenberg, C. E. *Electronic Processes in Organic Crystals and Polymers*, 2nd ed.; Oxford University Press: Oxford, 1999.